Data in Brief 48 (2023) 109086

Contents lists available at ScienceDirect

Data in Brief

journal homepage: www.elsevier.com/locate/dib

Data Article

Petrophysical and petrothermal dataset of the sedimentary succession in the Oliana anticline (Southern Pyrenees)

Pedro Ramirez-Perez[a,*], Irene Cantarero[a], Gabriel Cofrade[a], Daniel Muñoz-López[a], David Cruset[b], Jean-Pierre Sizun[c], Anna Travé[a]

[a] Grup Consolidat de Recerca Geologia Sedimentària, Departament de Mineralogia, Petrologia i Geologia Aplicada, Facultat de Ciències de la Terra, Universitat de Barcelona (UB), c/ Martí i Franquès s/n, Barcelona 08028, Spain
[b] Group of Dynamics of the Lithosphere, Geosciences Barcelona (GEO3BCN-CSIC), c/ Lluís Solé i Sabaris s/n, Barcelona 08028, Spain
[c] Chrono-Environnement, UMR CNRS 6249, Université de Franche-Comté, 16, Route de Gray, Besançon Cedex 25030, France

ARTICLE INFO

Article history:
Received 14 February 2023
Revised 15 March 2023
Accepted 17 March 2023
Available online 22 March 2023

Dataset link: Petrophysical and petrothermal raw data of the sedimentary succession in the Oliana anticline (Southern Pyrenees) (Original data)

Keywords:
Geothermal reservoir
Outcrop analogue
Alluvial succession
Permeability
Thermal conductivity

ABSTRACT

The petrophysical and petrothermal characterization of the sedimentary succession of the Oliana anticline in the Southern Pyrenees has been performed on the basis of mineral density, connected porosity, permeability, P-wave velocity and thermal conductivity measurements of rock samples distributed along this anticline. This dataset was used to explain: (I) the variability of petrophysical rock properties along the Oliana anticline, (II) the distribution of thermal conductivity along the sedimentary units of the anticline, (III) the relationships between the fold and petrology concerning the mineral density, connected porosity, permeability, P-wave velocity and thermal conductivity of rocks and (IV) the tectonic and diagenetic controls underlying the observed relationships, as described in the research article: "Petrological, petrophysical and petrothermal study of a folded sedimentary succession: the Oliana anticline (Southern Pyre-

DOI of original article: 10.1016/j.gloplacha.2023.104057
* Corresponding author.
E-mail address: pramirezperez@ub.edu (P. Ramirez-Perez).
Social media: @SedGeology_RG (P. Ramirez-Perez)

https://doi.org/10.1016/j.dib.2023.109086
2352-3409/© 2023 The Author(s). Published by Elsevier Inc. This is an open access article under the CC BY license (http://creativecommons.org/licenses/by/4.0/)

nees), outcrop analogue of a geothermal reservoir - Global and Planetary Change Journal (2023)".
This contribution presents here the raw and statistical datasets used to discuss the potential of the Oliana anticline as a geothermal reservoir analogue and also includes an extended methodological section that proposes a new procedure to measure the thermal conductivity of highly heterogeneous coarse-grained sedimentary rocks using the Modified Transient Source Plane (MTPS) method on a TCi C-Therm thermal analyzer.
These complete datasets can be used to better discuss and understand the principal limitations of outcrop analogue studies applied to unconventional geothermal reservoirs in foreland basins on the basis of the analysis of rock petrophysical and petrothermal properties. Furthermore, the data obtained in the Oliana anticline can be used to understand the structural, diagenetic and petrological factors that can modify the petrophysical and petrothermal properties of rocks and to discuss the potential of foreland basin margins to be used as geothermal reservoirs, comparing the data obtained in Oliana with studies developed in similar geological settings worldwide.

© 2023 The Author(s). Published by Elsevier Inc.
This is an open access article under the CC BY license (http://creativecommons.org/licenses/by/4.0/)

Specifications Table

Subject	Earth Sciences
Specific subject area	Petrophysics, petrothermics and petrology
Type of data	Tables Figures
How the data were acquired	Mineral and bulk density of sedimentary rocks were measured using the Archimedes method and calculated from mass and volume relations with an analytical accuracy of ± 0.002 g/cm^3. Connected porosity of sedimentary rocks was measured using the Archimedes method by water porosimetry, with an absolute accuracy of $\pm 0.05\%$. Permeability of sedimentary rocks was measured using a nitrogen gas permeameter equipped with a Hassler cell, using nitrogen and following a steady-state flow method. Results were corrected from Klinkenberg's effect using the graphical method. Analytical accuracy is $\pm 10\%$ (for K$\approx$1 D) and $\pm 0.5\%$ (for K$\approx$0.001 mD), detection threshold was 0.001 mD. P-wave velocity of sedimentary rocks was measured on water-saturated rocks using a portable Pundit 6 system (CNS Electronics LTD) operating at a regular frequency of 1 MHz. Absolute accuracy values range between ± 13 - 96 ms^{-1}. Thermal conductivity of detrital, carbonate and evaporite rocks was measured with a C-Therm Trident TCi thermal analyzer and the Modified Transient Plane Source (MTPS) method following ASTM D7984-21 measurement protocol. Statistical data has been processed using Excel and SPSS free software on raw measuring data. Please refer to the original research article and Experimental Design, Materials and Methods section for more detailed information on methodological protocols used for collecting data.
Data format	Raw and Analyzed

(*continued on next page*)

Description of data collection	Petrophysical and petrothermal properties are measured on samples collected during fieldwork in the Oliana anticline. Samples were processed at Universitat de Barcelona and in the Chrono-Environnement laboratory (PEA^{2}t platform) at Université de Franche-Comté to perform the different analyses (further information is included in the Experimental design, materials and methods section).
Data source location	The studied samples were collected from sedimentary formations cropping out at the northern limb, the southern limb, the NE closure and the SW closure of the Oliana anticline (Southern Pyrenees). The coordinates and location of each sample are included in Table 1 and Fig. 1, respectively. Samples are stored at Facultat de Ciències de la Terra, Universitat de Barcelona (UB), Martí i Franqués s/n, Barcelona, 08028, Spain.
Data accessibility	Data within the article Repository Repository name: Petrophysical and petrothermal raw data of the sedimentary succession in the Oliana anticline (Southern Pyrenees), [1] Data identification number: 10.17632/23zgg8rtb2.1 Direct URL to data: https://data.mendeley.com/datasets/23zgg8rtb2
Related research article	P. Ramirez-Perez, I. Cantarero, G. Cofrade, D. Muñoz-López, D. Cruset, J.P. Sizun, A. Travé, Petrological, petrophysical and petrothermal study of a folded sedimentary succession: the Oliana anticline (Southern Pyrenees), outcrop analogue of a geothermal reservoir. Global and Planetary Change (2023), 10.1016/j.gloplacha.2023.104057, [2]

Value of the Data

- Raw and statistical datasets are presented on petrophysical and petrothermal properties measured in carbonate and detrital rocks from the well-exposed Oliana anticline located on the northern margin of the Ebro foreland Basin, at the front of the Montsec and Serres Marginals thrust sheets (Southern Pyrenees).
- The article includes an extended and detailed description of the sampling and methodological procedures used to obtain representative values of thermal conductivity in coarse-grained sedimentary rocks of heterogeneous composition, such as conglomerates and coarse-grained sandstones. Statistical treatment of the original laboratory and field data is also provided.
- This type of study can be used by geoscientists working on geothermal reservoir characterization to improve the workflow used in their analyses and to better understand the limitations and advantages of statistical data studies applied to the investigation of geothermal reservoirs based on outcrop analogues.

1. Objective

The data presented here correspond to mineral density, bulk density, connected porosity, permeability and P-wave acoustic velocity of 40 sedimentary rocks and thermal conductivity data of 35 samples. The main objective of this article is to provide researchers with a more precise and complete scope of the results, analyses and workflow performed during the characterization of the folded alluvial succession of the Oliana anticline as an outcrop analogue of a geothermal reservoir located in the proximal margin of a foreland basin. Thus, all the datasets (raw and statistically processed) and procedures included here were used in the original research article [2]. The aim of this article is threefold 1) to provide a clearer picture of the analytical and statistical data processing of the results, 2) to extend the petrophysical and petrothermal dataset of the sedimentary succession studied in the Oliana anticline and 3) to present an extended sampling methodology and measurement procedure to acquire thermal conductivity data from petrologically heterogeneous rocks, which due to their grain size and compositional variability are challenging to be represented by a single value.

2. Data Description

The analysis of the petrophysical and petrothermal data from the sedimentary succession of the Oliana anticline (Southern Pyrenees) is presented here. Rock samples were collected from all the structural domains of the Oliana anticline covering the northern limb, the southern limb, the NE closure and the SW closure of the fold. The location, structural domain, geological age and lithofacies of each sample are shown in Table 1. Raw petrophysical and petrothermal data of samples are included in the Repository [1]. The statistical parameters on measured petrophysical properties (i.e., mineral density, bulk density, connected porosity, permeability and P-wave velocity) are displayed in Table 2 and the statistical descriptors on thermal conductivity are in Table 3. Fig. 1 displays a geological map of the Oliana anticline and the sampling location described in Table 1; Fig. 2 summarizes the statistical results as a function of the structural domains of the anticline and the sedimentary units; Fig. 3 displays the analytical variability of each property measured in the study by comparing the bedding perpendicular and bedding parallel values measured on the same sample, difference ratios between plugs are included in Table 4. The main stratigraphic and tectonic features of the Oliana anticline are described in [3–5], whereas the age of the sampled units has been constrained according to [6,7].

The folded sedimentary succession of the Oliana anticline includes marine marls in the core of the structure, limestones and evaporites in the transition from the core to the fold limbs and detrital rocks forming the anticline limbs. Within these detrital rocks, conglomerates are more abundant at the northern limb, whereas sandstones are typically found at the southern limb of the anticline. Marine marls and limestones, included in the Igualada Fm. and Tossa Fm., respectively, are upper Bartonian to middle Priabonian in age; gypsum rocks, belonging to the Ódena Fm. are a marginal equivalent of the evaporites of Cardona Fm., middle Priabonian in age; and detrital rocks are upper Priabonian to Chattian in age [3–5].

The detrital succession forming the fold limbs has been subdivided into four synorogenic units that are coeval to the upper Eocene to lower Oligocene break-back reactivation of the Serres Marginals and Montsec thrust sheets [3]. These units were described in the northern limb

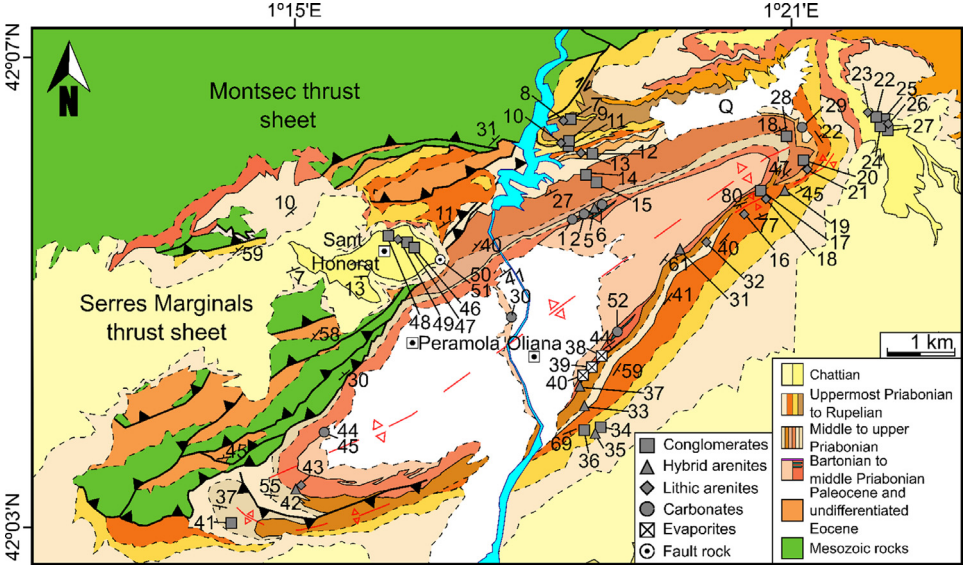

Fig. 1. Geological map of the Oliana anticline showing the studied lithofacies and the location of samples. More detailed information about samples is presented in Table 1. The cartography has been modified from [2].

Table 1
Location and lithofacies description of the studied sedimentary rocks. The geological age and the sector of the Oliana anticline are also displayed.

Location	Rock description	Sample	Synorogenic units	Latitude	Longitude
Northern limb (NL)	Fa-1. Coarse to fine-grained clast-supported conglomerates	PER7	U2 to 3 (uppermost Priabonian to Rupelian)	42° 6′ 44.79" N	1° 18′ 42.71" E
		PER9		42° 6′ 24.41" N	1° 18′ 45.72" E
		PER11		42° 6′ 24.41" N	1° 18′ 45.72" E
		PER12		42° 6′ 17.34" N	1° 18′ 57.90" E
		PER14	U1 (upper Priabonian)	42° 5′ 51.45" N	1° 19′ 11.15" E
		PER15		42° 5′ 49.93" N	1° 19′ 13.14" E
	Fa-2. Fossiliferous fine-grained hybrid arenites	PER2	Core (middle Priabonian)	42° 5′ 31.68" N	1° 19′ 8.22" E
		PER5	Transition from Core to U1 (middle Priabonian)	42° 5′ 21.77" N	1° 18′ 46.59" E
	Fa-3. Grauwackes	PER8	U2 to 3 (uppermost Priabonian to Rupelian)	42° 6′ 44.79" N	1° 18′ 42.71" E
		PER10		42° 6′ 24.41" N	1° 18′ 45.72" E
	Fa-3. Fine-grained lithic arenite	PER13		42° 6′ 17.34" N	1° 18′ 57.90" E
	Fa-4. Coral and nummulitic grainstones (Tossa Fm.)	PER1	Core (middle Priabonian)	42° 5′ 21.83" N	1° 18′ 46.57" E
	Fa-4. Coral and algal grainstone to packstone with nummulites (Terminal Complex)	PER6	Transition from Core to U1 (middle Priabonian)	42° 5′ 31.68" N	1° 19′ 8.22" E
	Fa-4. Marls with some quartz content (Igualada Fm.)	PER30	Core (middle Priabonian)	42° 4′ 16.91" N	1° 17′ 51.48" E
Sant Honorat (NL)	Fa-1. Microconglomerate to medium-grained conglomerates	PER46	U4 (Rupelian to Chattian)	42° 4′ 56.02" N	1° 16′ 26.55" E
		PER47		42° 4′ 57.04" N	1° 16′ 25.80" E
	Fa-3. Fine to medium-grained lithic arenites	PER48		42° 5′ 1.47" N	1° 16′ 12.61" E
		PER49		42° 4′ 57.13" N	1° 16′ 19.12" E
	Fault-rock	PER50	Serres Marginals thrust	42° 4′ 45.84" N	1° 16′ 54.49" E
		PER51			

(*continued on next page*)

Table 1 (*continued*)

Location	Rock description	Sample	Synorogenic units	Latitude	Longitude
NE closure (NEC)	Fa-1. Microconglomerates to medium-grained conglomerates	PER20	U1 (upper Priabonian)	42° 6′ 1.15" N	1° 22′ 11.43" E
		PER28		42° 6′ 15.27" N	1° 21′ 50.16" E
		PER22	U4 (Rupelian to Chattian)	42° 6′ 30.89" N	1° 23′ 13.29" E
		PER24		42° 6′ 24.92" N	1° 23′ 22.09" E
		PER25		42° 6′ 24.49" N	1° 23′ 22.57" E
		PER27		42° 6′ 24.39" N	1° 23′ 22.67" E
	Fa-3. Medium to coarse-grained lithic arenites	PER21	U2 (uppermost Priabonian)	42° 6′ 1.24" N	1° 22′ 11.61" E
		PER23	U4 (Rupelian to Chattian)	42° 6′ 30.68" N	1° 23′ 13.65" E
		PER26		42° 6′ 24.49" N	1° 23′ 22.57" E
	Fa-4. Wackestone with quartz	PER29	U1-2 (upper to uppermost Priabonian)	42° 6′ 26.46" N	1° 22′ 20.77" E
Southern limb (SL)	Fa-1. Microconglomerates to medium-grained conglomerates	PER17	U2 (uppermost Priabonian)	42° 5′ 30.71" N	1° 21′ 11.95" E
		PER34	U3 (Rupelian)	42° 3′ 1.52" N	1° 18′ 53.23" E
		PER36		42° 3′ 0.96" N	1° 18′ 43.89" E
	Fa-2. Very fine to fine-grained hybrid arenites	PER31	Core (middle Priabonian)	42° 5′ 0.81" N	1° 20′ 14.94" E
		PER37	U1 (upper Priabonian)	42° 5′ 46.45" N	1° 21′ 58.41" E
		PER19	U1-2 (upper to uppermost	42° 3′ 18.96" N	1° 18′ 45.97" E
		PER33	Priabonian)	42° 3′ 30.38" N	1° 18′ 43.00" E
		PER35	U3 (Rupelian)	42° 3′ 1.43" N	1° 18′ 52.39" E
	Fa-3. Fine to medium-grained lithic arenites	PER16	U2 (uppermost Priabonian)	42° 5′ 28.63" N	1° 21′ 9.79" E
		PER18		42° 5′ 29.22" N	1° 21′ 13.35" E
		PER32	U1 (upper Priabonian)	42° 5′ 1.67" N	1° 20′ 40.37" E
	Fa-4. Nummulitic packstone	PER52	Core (middle Priabonian)	42° 4′ 4.22" N	1° 19′ 7.48" E
	Fa-5. Gypsum mixed with lutites (Ódena Fm.)	PER38	Transition from Core to U1	42° 3′ 39.66" N	1° 18′ 48.65" E
		PER39	(middle Priabonian)	42° 3′ 43.18" N	1° 18′ 51.77" E
		PER40		42° 3′ 35.45" N	1° 18′ 46.95" E
SW closure (SWC)	Fa-1. Medium -grained conglomerates	PER41	U1 (upper Priabonian)	42° 2′9.42"N	1° 14′ 34.44" E
	Fa-2. Coarse-grained hybrid arenites	PER42	Transition from Core to U1	42° 2′ 26.03" N	1° 15′ 19.75" E
	Fa-3. Fine-grained lithic arenites	PER43	(middle Priabonian)	42° 2′ 27.00" N	1° 15′ 19.41" E
	Fa-4. Wackestone with quartz	PER44	Core (middle Priabonian)	42° 2′ 59.53" N	1° 15′ 28.53" E
		PER45			

Table 2
Statistical data on the petrophysical properties measured in the Oliana anticline. Arithmetic mean ($\dot{x}$), median (Me), variance (s) and Coefficient of Variation (CV) of mineral density (ρ_{min}), bulk density (ρ_{bulk}), connected porosity (N_t), permeability (K) and P-wave velocity (v_p) are displayed attending to the fold sector (above) and the sedimentary unit (below). 62 values from 40 samples are resumed.

Location	Number of values (Number of samples)	ρ_{min}				ρ_{bulk}			
		$\dot{x}$ (g/cm^3)	Me (g/cm^3)	s (g/cm^3)	CV (%)	$\dot{x}$ (g/cm^3)	Me (g/cm^3)	s (g/cm^3)	CV (%)
NL	22 (15)	2.716	2.720	± 0.024	1	2.582	2.623	± 0.112	4
SL	23 (13)	2.686	2.705	± 0.083	3	2.548	2.573	± 0.095	4
NEC	12 (8)	2.710	2.708	± 0.014	1	2.585	2.584	± 0.053	2
SWC	5 (4)	2.706	2.713	± 0.021	1	2.345	2.204	± 0.274	12

Location	Number of values (Number of samples)	N_t				K			
		$\dot{x}$ (%)	Me (%)	s (%)	CV (%)	$\dot{x}$ (mD)	Me (mD)	s (mD)	CV (%)
NL	22 (15)	4.81	3.37	± 4.32	90	25.62	0.086	± 92.20	>100
SL	23 (13)	5.11	3.77	± 3.04	59	0.481	0.053	± 0.938	
NEC	12 (8)	4.60	4.44	± 2.22	48	29.52	0.228	± 92.12	
SWC	5 (4)	13.92	19.69	± 9.79	70	31.91	0.316	± 44.38	

Location	Number of values (Number of samples)	V_p			
		$\dot{x}$ (ms^{-1})	Me (ms^{-1})	s (ms^{-1})	CV (%)
NL	22 (15)	4533	4433	± 1022	23
SL	23 (13)	4644	5046	± 776	17
NEC	12 (8)	4238	4955	± 1003	24
SWC	5 (4)	3311	2880	± 1205	36

Unit	Number of values (Number of samples)	ρ_{min}				ρ_{bulk}			
		$\dot{x}$ (g/cm^3)	Me (g/cm^3)	s (g/cm^3)	CV (%)	$\dot{x}$ (g/cm^3)	Me (g/cm^3)	s (g/cm^3)	CV (%)
Core	12 (8)	2.677	2.704	± 0.109	4	2.420	2.511	± 0.209	9
U1	15 (9)	2.697	2.698	± 0.038	1	2.594	2.604	± 0.090	3
U2-3	27 (17)	2.715	2.713	± 0.024	1	2.580	2.596	± 0.081	3
U4	8 (6)	2.722	2.724	± 0.009	0.3	2.569	2.571	± 0.051	2

Unit	Number of values (Number of samples)	N_t				K			
		$\dot{x}$ (%)	Me (%)	s (%)	CV (%)	$\dot{x}$ (mD)	Me (mD)	s (mD)	CV (%)
Core	12 (8)	9.47	6.13	± 0.427	85	17.97	0.053	± 35.44	>100
U1	15 (9)	3.66	2.52	± 0.284	96	29.39	0.075	± 92.17	
U2-3	27 (17)	4.99	3.71	± 0.219	62	18.09	0.096	± 78.52	
U4	8 (6)	5.61	5.63	± 0.092	30	2.15	0.266	± 5.12	

Unit	Number of values (Number of samples)	V_p			
		$\dot{x}$ (ms^{-1})	Me (ms^{-1})	s (ms^{-1})	CV (%)
Core	12 (8)	4225	4632	± 1384	33
U1	15 (9)	4986	5288	± 751	15
U2-3	27 (17)	4354	4472	± 832	19
U4	8 (6)	3862	3862	± 860	22

of the anticline considering the relationship between the main thrusts and the conglomerates at their footwall [4]. In this sense, Unit 1 is of middle to upper Priabonian in age; Unit 2 is of uppermost Priabonian and Unit 3 is of Rupelian in age. Unit 4 fossilizes all the previous synorogenic units and is dated as Rupelian to Chattian. The samples from the sedimentary succession of the Oliana anticline were grouped into five main lithofacies (Fa-1 to Fa-5) including

Table 3
Statistical data on the thermal conductivity measured at the Oliana anticline. Arithmetic mean (ẋ), median (Me), variance (s) and Coefficient of Variation (CV) are displayed attending to the fold sector and the sedimentary unit . 55 values from 35 samples are resumed in both cases.

Unit	Number of values (Number of samples)	τ ($Wm^{-1}K^{-1}$)			
		ẋ ($Wm^{-1}K^{-1}$)	Me ($Wm^{-1}K^{-1}$)	s ($Wm^{-1}K^{-1}$)	CV (%)
NL	19 (12)	3.157	3.232	± 0.315	10
SL	18 (13)	3.137	3.185	± 0.40	13
NEC	15 (8)	3.326	3.341	± 0.156	5
SWC	3 (2)	3.036	2.813	± 0.495	16
Unit	Number of values (Number of samples)	τ ($Wm^{-1}K^{-1}$)			
		ẋ ($Wm^{-1}K^{-1}$)	Me ($Wm^{-1}K^{-1}$)	s ($Wm^{-1}K^{-1}$)	CV (%)
Core	8 (5)	2.705	2.752	± 0.427	16
U1	14 (9)	3.313	3.393	± 0.284	9
U2-3	24 (15)	3.238	3.249	± 0.219	7
U4	9 (6)	3.303	3.257	± 0.092	3

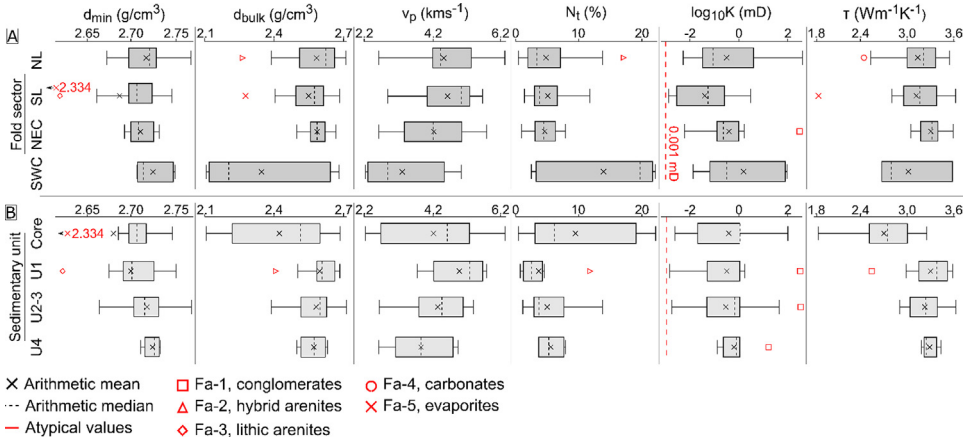

Fig. 2. Statistical summary of the studied properties sorted by fold sectors (a) and by sedimentary units (b) of the Oliana anticline. The figure allows to compare different tendencies explained in the text and observed between the structural sectors and the stratigraphy. The arithmetic mean and median are displayed in the diagrams. The number of values in each box are presented in Tables 2 and 3. C=Core, U1 to U4=synorogenic units 1 to 4.

conglomerates, hybrid arenites, lithic arenites, carbonates and evaporites [2]; other samples collected but not analyzed due to experimental limitations (i.e., fault rocks) are also included in Table 1.

Petrophysical data have been analyzed by statistical descriptors such as coefficient of variation (CV), arithmetic mean (ẋ), arithmetic median (Me) and variance (s) to assign a representative value to the different fold sectors, lithostratigraphic units and lithofacies of the Oliana anticline, information necessary to build a geothermal reservoir model (Table 2). 62 values were acquired for each property (mineral density, bulk density, connected porosity, permeability and P-wave velocity). A graphical summary of these data sorted by fold sectors is shown in Fig. 2a and by sedimentary units of the Oliana anticline in Fig. 2b.

The coefficient of variation (CV) is a statistical descriptor that allows to establish the data scattering with respect to the arithmetic mean (ẋ). A CV greater than 50% indicates that more than half of the measured values differ significantly from the calculated mean. Commonly, a value of 30% is used as a cut-off to consider whether the correlation between the measured data

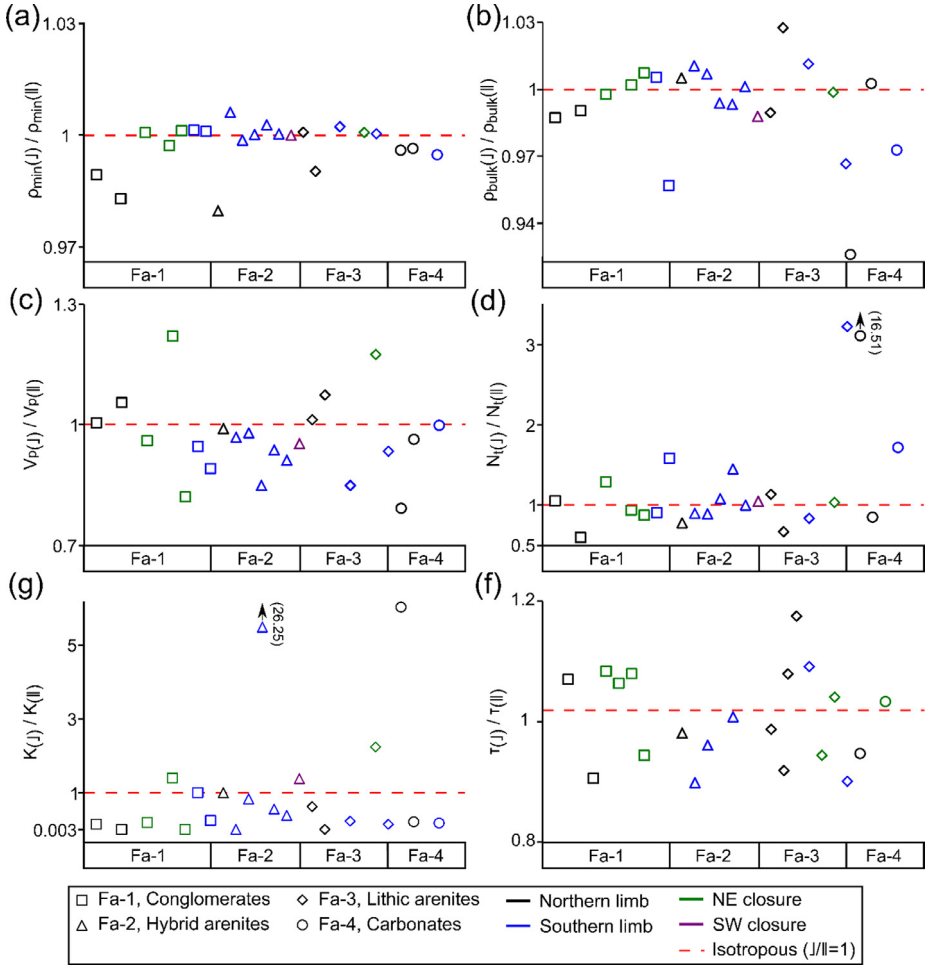

Fig. 3. Petrological heterogeneity of (a) mineral density, (b) bulk density, (c) P-wave velocity, (d) connected porosity, (e) permeability and (f) thermal conductivity attending to the lithofacies. Graphs a to e summarize 62 measures from 40 samples. Graph f shows 55 measures from 35 samples (Table 4).

and the arithmetic mean is good or not. Thus, low CV values indicate that the arithmetic mean is representative of the property. In contrast, for values above 30%, the arithmetic median (Me) should be used as the mean value of the property. The variance (s) is a statistical descriptor that represents, with a numerical value, the average absolute variation of the measures with respect to the arithmetic mean.

Considering the studied properties, mineral density presents a low CV in all the fold sectors, which means that the results are little variable. Therefore, the calculated average mineral density is statistically representative of the different fold sectors. In the case of bulk density, a slight increase in CV is observed. However, it is far from the value of 30%, which means that even if the data are more dispersed than for mineral density, the calculated arithmetic means are still representative of the bulk density of each fold sector. A comparison of the density data across the anticline reveals that the northern limb and NE closure are denser than the southern limb and SW closure of the fold (Fig. 2a). This observation also coincides with the predominance of

coarser-grained lithofacies in the northern limb and NE closure (i.e., conglomerates and microconglomerates) than in the remaining sectors of the fold (mainly sandstones).

The coefficient of variation of connected porosity (48 to 90%), permeability (CV greater than 100%) and P-wave velocity (17 to 36%) indicates that these properties are much more variable than mineral and bulk densities. However, the CV values of P-wave velocity indicate that this property, although highly variable, can be characterized along the anticline based on the calculated mean values. In this sense, the arithmetic mean calculated for the SW closure has a lower representativeness due to high CV value (Table 2). Even so, the measured P-wave velocities are comparatively lower in this sector of the Oliana anticline than in the others (Fig. 2a). Attending to the connected porosity and permeability, it is not correct to use the arithmetic means to characterize them. Instead, the arithmetic median should be used for this purpose.

The comparison of the median of connected porosity along the fold sectors of the Oliana anticline reveals that the lowest pore connectivity is measured in the northern limb, followed by the southern limb, the NE and the SW closures of the fold (Fig. 2a). In this respect, higher scattering of the measurements has been detected in the northern limb (CV=90%). The arithmetic median of permeability shows that the SW closure is the most permeable sector, followed by the NE closure and the northern and southern limbs of the Oliana anticline. However, due to the high scatter of the data (CV>100%), these results would be unrepresentative of the real rock permeability in the studied sectors.

Attending to the sedimentary units (Fig. 2b), the core of the Oliana anticline displays the greatest dispersion of values for all measured properties except for mineral density. Comparatively, the detrital synorogenic units are less variable. Among these units, synorogenic Unit 1 shows the highest mean bulk density (CV=3%) and the lowest connected porosity and permeability, considering in both cases the arithmetic median due to the high CV values for these properties (96% and >100%, respectively, Table 2). Synorogenic Units 2 and 3 (U2-3) show the highest variations within the detrital succession, while Units 1 and 4 are well clustered for almost all the studied properties.

The statistical descriptors of the thermal conductivity are shown in Table 3. The CV of the thermal conductivity indicates that the data are well clustered in the different sectors and stratigraphic units of the Oliana anticline (in both cases the measured CV values are lower than 20%). In this sense, the thermal conductivity of the different fold sectors is less variable than that of the sedimentary units (Fig. 2).

In the Oliana anticline, major changes in thermal conductivity measurements are observed considering the different sedimentary units rather than the fold sectors; thus, the average thermal conductivity in the different fold sectors varies from 3.036 to 3.326 $Wm^{-1}K^{-1}$, whereas it ranges from 2.705 to 3.313 $Wm^{-1}K^{-1}$ when comparing the sedimentary units. The lowest thermal conductivities are measured in samples from the more carbonate and evaporitic sectors of the fold (i.e., the SW closure and the core unit), whereas higher thermal conductivities are measured in the fold limbs coinciding with a more detrital composition. In addition, a change in thermal conductivity between the four tectonosedimentary detrital units is observed, being the mean thermal conductivity of Units 1 and 4 (3.313 and 3.303 $Wm^{-1}K^{-1}$, respectively) higher than for Units 2 and 3 (3.238 $Wm^{-1}K^{-1}$) due to the different composition of the detrital rocks of each unit [2].

Table 4 displays the variations of these properties for each lithofacies (Fa-1 to Fa-5). The difference ratios (d) of the studied properties have been obtained dividing the values acquired from bed-perpendicular plugs by the values obtained from bed-parallel plugs in the same sample. Fig. 3 shows graphs summarizing the petrophysical and petrothermal differences observed in the studied rocks. These data also illustrate the heterogeneity of properties along the different facies, which would be of interest for reservoir characterization. In this regard, an isotropous specimen would have a value of 1, whereas this value is higher if the bed-perpendicular measurement is greater than the value acquired from the plug oriented parallel to the bedding. Otherwise, the obtained value is less than 1.

Mineral density, bulk density and P-wave velocity are little heterogeneous (the maximum difference ratio with respect to 1 is 0.980 for mineral density; is 0.931 for bulk density and 1.220

Table 4
Difference ratios (d) for each studied property obtained by comparing bed-parallel and bed-perpendicular measurements of the same sample. Isotropous rocks display a value of 1.

Facies	Sample	Property difference ratio (d)					
		τ	ρ_{min}	ρ_{bulk}	N_t	K	v_p
Fa-1, conglomerates	PER7	-	0.989	0.988	1.050	0.140	1.004
	PER9	1.051	-	-	-	-	-
	PER12	-	0.983	0.991	0.595	0.010	1.054
	PER15	0.886	-	-	-	-	-
	PER20	1.064	1.001	0.998	1.289	-	0.960
	PER24	1.044	-	-	-	-	-
	PER27	1.060	0.997	1.002	0.934	1.396	1.220
	PER28	0.924	1.001	1.007	0.872	0.005	0.820
	PER34	-	1.001	1.005	0.903	1.00	0.946
	PER36	-	1.001	0.960	1.584	0.247	0.890
Fa-2, hybrid arenites	PER5	0.961	0.980	1.005	0.773	-	0.990
	PER19	0.879	1.006	1.010	0.895	-	0.968
	PER31	0.941	0.999	1.006	0.888	0.821	0.978
	PER33	-	1.00	0.994	1.071	26.250	0.848
	PER35	0.989	1.003	0.993	1.445	-	0.936
	PER37	-	1.00	1.001	0.995	0.393	0.910
	PER42	-	1.00	0.989	1.042	1.382	0.951
Fa-3, lithic arenites	PER8	0.968	1.001	0.990	1.128	0.632	1.011
	PER10	0.899	0.990	1.025	0.665	0.010	1.073
	PER13	0.865	-	-	-	-	-
	PER16	1.072	1.002	1.010	0.827	0.236	0.848
	PER21	0.925	-	-	-	-	-
	PER23	1.021	1.001	0.998	1.026	2.218	1.173
	PER32	0.881	1.00	0.969	3.221	-	0.933
	PER43	0.957	-	-	-	-	-
Fa-4, carbonates	PER1	0.928	0.996	0.931	16.508	-	0.791
	PER6	-	0.996	1.002	0.844	0.220	0.963
	PER29	1.013	-	-	-	-	-
	PER52	-	0.995	0.975	1.718	-	0.998

for P-wave velocity, Fig. 3a-c). In contrast, the results for connected porosity and permeability change significantly in the same sample depending on the measurement orientation (the maximum difference ratios are 16.51 and 26.25, Fig. 3c-e).

In this respect, whereas the anisotropy observed for mineral density, bulk density, P-wave velocity and connected porosity is intrinsically linked to the variability of the measurement within the plug, the anisotropy of transfer properties such as permeability and thermal conductivity are of special interest at time of performing the geothermal reservoir modelling and are strongly dependent of the petrographic heterogeneities of the rock such as the texture or the grain fabric. Therefore, in case of permeability, this property is detected to be highly anisotropous among the measurement orientation, especially regarding to hybrid arenites and limestones that display the greatest heterogeneity values acquired in the same sample. Thereby, permeability is expected to be difficult to upscale using the data collected from the 40 studied samples to the entire sedimentary succession of the Oliana anticline, especially in the case of limestones due to the strong data scattering depending on the measure direction with respect to bedding.

Considering the petrothermal characterization of the Oliana anticline, the samples show little thermal heterogeneity. The maximum difference ratio between measurements taken parallel and perpendicular to the bedding strike is 0.865 (Fig. 3f). Consequently, although the thermal conductivity of the parallel and perpendicular plugs is slightly different, this property could be upscaled to the sedimentary succession of the Oliana anticline using the data presented in this contribution and considering the corresponding lithofacies.

3. Experimental Design, Materials and Methods

The methodology of the petrological description of the samples in Oliana has just been explained in the original research article [2]. Details on the acquisition of petrophysical data can be found in [8,9]. This section adds information about the sampling design and treatment of the samples before measuring their petrophysical and petrothermal properties. In addition, an extended methodological description of the petrothermal measurement design for highly heterogeneous rock samples and the subsequent statistical study of the data is also presented.

Fieldwork has been carried out during five days in June 2020. Rock samples were oriented in the field with respect to the bedding strike and collected throughout the Oliana anticline to cover the different stratigraphic units and sectors of the structure. In this sense, the sampling was designed to guarantee a representativeness of the collected rocks with respect to the stratigraphic succession of the Oliana anticline. Collected samples were also checked for ensure that do not present any visible alteration and that they were of an adequate size to allow the acquisition of the different rock pieces necessary for the collection of the data.

In addition, as one of the objectives of this study was to analyse whether structural factors affect the thermal and physical properties of the rocks, samples were taken in all the sectors of the Oliana anticline (i.e., the NE and SW closures and the northern and southern limbs). Twenty samples were taken from the northern limb, fifteen from the southern limb, ten from the NE closure and five from the SW closure of the fold. In total, 50 samples were acquired for their petrological, petrophysical and petrothermal characterization (Table 1).

Before laboratory measurements, samples were photographed, marked and then sawn to perform rock cubes of a minimum dimension of $5.0 \times 5.0 \times 7.0$ m, which is the volume that allows the drilling of 4.0×5.5 cm cylindrical plugs. These plugs were used to measure mineral and bulk density, connected porosity, permeability and P-wave velocity of the rocks. The dimensions of the cylindrical plugs were decided on the basis of ensuring a Representative Elementary Volume of rock during the measurement of each petrophysical property. In addition, plug dimensions were limited by the Hassler cell size of the permeameter. The petrophysical results presented in this contribution represent the properties of 62 plugs from 40 samples; 36 values were parallel to the bedding, whereas 26 values were perpendicular to it.

Samples were also sawn into slices parallel and perpendicular to the bedding surface. These slices have a minimum thickness of 3 cm to avoid heat dispersion out of the sample and two smooth and parallel surfaces to place the thermal sensor and measure the rock thermal conductivity. The horizontal dimensions of the slices depended on the observed petrological heterogeneity, as the aim was to obtain the most representative surfaces for their measurement. The thermal characterization of the Oliana anticline was carried out considering the thermal conductivity results of 55 slices from 35 samples. 24 slices were parallel to the bedding, whereas 31 slices were perpendicular to it.

Petrothermal results were acquired using a TCi C-Therm Trident thermal analyzer, implemented with the Modified Transient Plane Source (MTPS) method [10–12]. This device applies an electric pulse to the sample with a variable voltage ranging from 110 to 230 V, depending on the initial temperature at the rock-sensor interphase. A one-sided heat reflectance sensor surrounded by an insulative piece applies a short electric pulse to the measured sample. The pulse is so short that the specimen is considered to be in contact with an infinite solid of high conductivity during the measurement. The applied electric voltage generates a slight thermal gradient which causes a heat transfer between the rock and the heating sensor. As the heating point is small and thermally insulated, the heat exchange between the specimen and the sensor is assumed to occur in a 1D space, ensuring that no external factor or heat loss affects the experiment.

The thermal properties of the specimen are calculated by recording the change in voltage over the measuring time, which is automatically set considering that the sample boundaries do not affect the temperature raise caused by the electric pulse. During the measurement time, the temperature of the rock-sensor interphase raises by 1 ºC. The rock sample absorbs the heat

generating a simultaneous voltage drop. The petrothermal properties are calculated from the slope resulting from plotting the voltage variation versus measuring time.

Samples were dried in an oven by at least 24 h at 70 ºC and were then temperate for other 24 ± 6 h in stable temperature (22 ± 3 ºC) and moisture (52 ± 14%) room conditions. Temperature and moisture were also periodically checked to ensure controlled conditions while measuring (see data in Repository). Before each measurement the sensor was calibrated using reference polymer and pyroceramic test materials. Distilled water was applied as a contact agent between the sample and the sensor. The surface area of the sensor is limited and, as the thermal conductivity is measured by placing the sensor directly over the rock slices, the values acquired are not representative of the whole rock when the sample is heterogeneous. Instead, they are representative of the thermal conductivity of the measured point. To overcome this, in the case of petrologically heterogeneous samples, the sensor was randomly placed at different points of the surface, usually from 2 to 6 points were measured on each slice (see data in Repository). For each point a cycle of 2 to 3 simultaneous measurements was run to acquire, in the end, a total of 12 values for each slice. After each cycle, the Trident software displays an average thermal conductivity value of the measured point and its Relative Standard Deviation (RSD). RSD must always be less than 1 to comply with the technical considerations of measurement methodology (ASTM D7984-21).

Finally, a single, representative value of the thermal conductivity for each sample was calculated by averaging the results of all the measured points in the slice. The RSD value obtained after averaging all the points must also be less than 1, so the raw data were statistically treated to delete from the cycles the values that place the RSD above the methodological threshold. After this process, a single thermal conductivity value is acquired, which is technically correct and representative of the measured sample because it respects the petrological heterogeneity of the rock. This measuring procedure has been widely implemented in the case of conglomerates and some coarse to medium-grained sandstones of the Oliana anticline.

The statistical treatment of the raw petrophysical and petrothermal data was carried out using the free SPSS software and Microsoft Excel to calculate the statistic descriptors presented in Tables 2–4 of this contribution. Simple arithmetic functions were used to calculate the arithmetic mean ($\dot{x}$), arithmetic median (Me), variance (s), coefficient of variation (CV) and difference (d) of each studied property. The graphs shown in Figs. 1 and 2 were also produced by Microsoft Excel and then remastered using Inkscape free vectorial drawing program.

Ethics Statements

The authors declare that this work meets the ethical requirements established by the journal and that does not involve studies with animals and humans.

Declaration of Competing Interest

The authors declare that they have no known competing financial interests or personal relationships that could have appeared to influence the work reported in this paper.

Data Availability

Petrophysical and petrothermal raw data of the sedimentary succession in the Oliana anticline (Southern Pyrenees) (Original data) (Mendeley Data).

CRediT Author Statement

Pedro Ramirez-Perez: Conceptualization, Investigation, Methodology, Formal analysis, Data curation, Writing – original draft, Writing – review & editing; **Irene Cantarero:** Conceptualization, Investigation, Supervision, Methodology, Formal analysis, Validation; **Gabriel Cofrade:** Visualization, Formal analysis; **Daniel Muñoz-López:** Conceptualization, Investigation, Data curation, Resources; **David Cruset:** Data curation, Formal analysis; **Jean-Pierre Sizun:** Investigation, Methodology, Validation, Formal analysis, Visualization; **Anna Travé:** Conceptualization, Investigation, Supervision, Formal analysis, Validation, Visualization, Project administration, Funding acquisition.

Acknowledgments

This research was performed within the framework of DGICYT Spanish Project PGC2018-093903-B-C22 and PID2021-12246NB-C22 Ministerio de Ciencia, Innovación y Universidades/Agencia Estatal de Investigación/Fondo Europeo de Desarrollo Regional and the Catalan Council to the Grup Consolidat de Recerca Reconegut Geologia Sedimentària (2021 SGR-Cat 00349).

DC acknowledges the Spanish Ministry of Science and Innovation for the "Juan de la Cierva Formación" fellowship FJC2020-043488-I AEI/10.13039/501100011033.

PR acknowledges the Universitat de Barcelona and Repsol Exploración. S.A. for the "Repsol-UB 2020" fellowship D/226000900/C2022A/G00/ PDZJK002 and the Universitat de Barcelona for the "PREDOC-UB 2021" fellowship.

References

[1] P. Ramirez-Perez, Petrophysical and petrothermal raw data of the sedimentary succession in the Oliana anticline (Southern Pyrenees), Mendeley Data V1, (2023), doi:10.17632/23zgg8rtb2.1.
[2] P. Ramirez-Perez, I. Cantarero, G. Cofrade, D. Muñoz-López, D. Cruset, J.P. Sizun, A. Travé, Petrological, petrophysical and petrothermal study of a folded sedimentary succession: the Oliana anticline (Southern Pyrenees), outcrop analogue of a geothermal reservoir, Glob. Planet. Change (2023), doi:10.1016/j.gloplacha.2023.104057.
[3] J. Vergés, J.A. Muñoz, Thrust sequences in the southern central Pyrenees, Bull. La Société Géologique Fr. 4 (1990) 265–271, doi:10.2113/gssgfbull.VI.2.265.
[4] D.W. Burbank, J. Vergés, Reconstruction of topography and related depositional systems during active thrusting, J. Geophys. Res. 99 (1994) 281–297, doi:10.1029/94JB00463.
[5] A.J. Sussman, R.F. Butler, J. Dinarès-Turell, J. Vergés, Vertical-axis rotation of a foreland fold and implications for orogenic curvature: An example from the Southern Pyrenees, Spain, Earth Planet. Sci. Lett. 218 (2004) 435–449, doi:10.1016/S0012-821X(03)00644-7.
[6] E. Costa, M. Garcés, M. López-Blanco, E. Beamud, M. Gómez-Paccard, J.C. Larrasoaña, Closing and continentalization of the South Pyrenean foreland basin (NE Spain): magnetochronological constraints, Basin Res. 22 (2010) 904–917, doi:10.1111/J.1365-2117.2009.00452.X.
[7] M. Garcés, M. López-Blanco, L. Valero, E. Beamud, J.A. Muñoz, B. Oliva-Urcia, A. Vinyoles, P. Arbués, P. Cabello, L. Cabrera, Paleogeographic and sedimentary evolution of the South Pyrenean foreland basin, Mar. Pet. Geol. 113 (2020) 104105, doi:10.1016/J.MARPETGEO.2019.104105.
[8] J. Richard, J.P. Sizun, Pressure solution-fracturing interactions in weakly cohesive carbonate sediments and rocks: Example of the synsedimentary deformation of the Campanian chalk from the Mons Basin (Belgium), J. Struct. Geol. 33 (2011) 154–168, doi:10.1016/J.JSG.2010.11.006.
[9] T. Cavailhes, J.P. Sizun, P. Labaume, A. Chauvet, M. Buatier, R. Soliva, L. Mezri, D. Charpentier, H. Leclere, A. Trave, C. Gout, Influence of fault rock foliation on fault zone permeability: The case of deeply buried arkosic sandstones (Grès d'Annot, southeastern France), Am. Assoc. Pet. Geol. Bull. 97 (2013) 1521–1543, doi:10.1306/03071312127.
[10] S.E. Gustafsson, Transient plane source techniques for thermal conductivity and thermal diffusivity measurements of solid materials, Rev. Sci. Instrum. 62 (1998) 797, doi:10.1063/1.1142087.
[11] E. Di Sipio, S. Chiesa, E. Destro, A. Galgaro, A. Giaretta, G. Gola, A. Manzella, Rock thermal conductivity as key parameter for geothermal numerical models, Energy Procedia 40 (2013) 87–94, doi:10.1016/J.EGYPRO.2013.08.011.
[12] M. Labus, K. Labus, Thermal conductivity and diffusivity of fine-grained sedimentary rocks, J. Therm. Anal. Calorim. 132 (2018) 1669–1676, doi:10.1007/s10973-018-7090-5.